IEEE *Access*

Multidisciplinary : Rapid Review : Open Access Journal

Flexible Kurtogram for Extracting Repetitive Transients for Prognostics and Health Management of Rotating Components

JINGJING ZHONG, JIANYU LONG, SHAOHUI ZHANG[iD]**, AND CHUAN LI**[iD]

College of Mechanical Engineering, Dongguan University of Technology, Dongguan 523808, China

Corresponding author: Chuan Li (chuanli@dgut.edu.cn)

ABSTRACT Rotating components are commonly used in industry and their failures may cause unexpected accidents and economic losses. To prevent these, prognostics and health management of rotating components attract much attention. The key for prognostics and health management of rotating components is to extract repetitive transients caused by early faults, which is further used to construct health indicators for describing rotating component degradation. In the past years, various theories and algorithms were developed to extract repetitive transients. One of the most famous theories is spectral kurtosis. Moreover, its fast realization is called fast Kurtogram. Even though several improvements have been made on spectral kurtosis and its fast realization, the fast Kurtogram is not an optimal filtering. In this paper, flexible Kurtogram is proposed. First, a flexible filtering framework based on multiple filter banks is constructed. Second, the objective functions of the flexible Kurtogram based on generalized spectral kurtosis are proposed. Third, optimization algorithms are introduced to maximize objective functions so as to make the flexible Kurtogram adaptive for the squared envelope with demodulation analysis. The results showed that the proposed flexible Kurtogram can be used to automatically find an optimal frequency band for demodulation analysis and it is better than the fast Kurtogram.

INDEX TERMS Flexible Kurtogram, optimal filtering, prognostics and health management, repetitive transients, rotating components.

I. INTRODUCTION

Rotating components, such as bearings and gears, are widely used in various machines in industry. Their health conditions are of great concern because unexpected failures of rotating components may cause further damages of other connected components and even cause failures of a whole transmission system [1], [2]. Prognostics and health management of rotating components aim to use monitoring data to timely determine health conditions of rotating components and make maintenance plans economic so as to prevent unexpected accidents and reduce economic losses [3].

Prognostics and health management of rotating components includes several steps, such as data collection, data processing, prognostic modeling and maintenance modeling [4].

The associate editor coordinating the review of this manuscript and approving it for publication was Dong Wang.

Among them, data processing is the key for construction of health indicators for prognostic modeling of rotating components. For example, when a bearing in a machine suffers a fault, repetitive transients are generated by rollers striking the fault. Because of interruptions of heavy noises and strong unwanted vibration components, repetitive transients are not directly observed in practice [5]. Consequently, it is difficult to directly use statistical parameters to quantify repetitive transients and reflect health conditions of rotating components. Here, statistical parameters can be understood as health indicators [6], which are used as an input to prognostic modeling. Simply speaking, health indicators are the basis of prognostic modeling [7]. In view of this point, extraction of repetitive transients is crucial to prognostics and health management of rotating components.

In the past years, in the field of mechanical signal processing, many theories and methods for extracting repetitive

transients were proposed [8]. Among them, spectral kurtosis [9] is one of the most famous theories to realize extraction of repetitive transients. Spectral kurtosis originally proposed by Antoni and Randall [10] aims to use kurtosis to quantify an analytical signal constructed by using a band-pass filter and Hilbert transform. Here, kurtosis is capable of characterizing the impulsiveness of repetitive transients. Therefore, spectral kurtosis can be used to extract repetitive transients with an assumption that there are no impulsive noises embedded in repetitive transients. Based on the theory of spectral kurtosis, the fast realization of spectral kurtosis was then proposed by Antoni and it was called the fast Kurtogram [11].

Following the work of Antoni, many improvements on spectral kurtosis and its fast realization were proposed [12]. Some examples are given as follows. Li *et al.* [13] proposed multiscale clustered grey infogram to reduce the influence of impulsive noises. Borghesani *et al.* [14] innovatively revealed that spectral kurtosis is proportional to the sum of the square of the squared envelope spectrum. Wang [15] discovered that spectral kurtosis is a special case of the ratio of *Lp* norm to *Lq* norm when $p = 2$ and $q = 1$. Moreover, Wang [15] connected spectral kurtosis with the reciprocal of spectral smoothness index [16]. Then, inspired by Gini index [17] and the work of Miao *et al.* [18], Wang [19] introduced Gini index to extract repetitive transients and developed spectral Gini index. Results showed that spectral Gini index and spectral smoothness index are less sensitive to impulsive noises. Here, in the work of Miao *et al.* [18], they used Gini index instead of kurtosis in the fast Kurtogram and showed that Gini index is less sensitive to impulsive noises. Mo *et al.* [20] discovered that a cyclic harmonic-to-noise ratio is a special case of the ratio of *Lp* norm to *Lq* norm when $p = +\infty$ and $q = 1$. Then, they proposed weighted cyclic harmonic-to-noise ratio to further improve the signal to noise ratio of the cyclic harmonic-to-noise ratio and made the proposed index more effective for extracting repetitive transients.

To characterize the cyclo-stationarity of repetitive transients, Barszcz and Jabłoński [21] used kurtosis to quantify the amplitudes of squared envelope spectrum and then they proposed the concept of the Protrugram. To expedite the calculation time of the Protrugram, Wang *et al.* [22] used kurtosis to quantify squared envelope spectra of wavelet packet coefficients and they called this technique as the enhanced Kurtogram. Antoni [23] used negative entropy to quantify squared envelope spectra. Besides, Antoni proposed an innovative idea to simultaneously characterize the impulsiveness and cyclo-stationarity of repetitive transients by using an average of negative entropies in time and frequency domains. Nevertheless, Antoni did not clarify how to set a weight of negative entropies in time and frequency domains. Wang *et al.* used the ratio of *L2* norm to *L1* norm [24] to quantify bearing fault frequencies in squared envelope spectra to find the most informative frequency band excited by bearing faults.

Besides characterizing the impulsiveness and cyclo-stationarity of repetitive transients, filtering for bearing fault diagnosis has attract much attention from scholars, which

is practical realizations of some theories. Qin [25] used a Laplace wavelet as a mother wavelet to realize sparse representation of bearing fault signals. Wang *et al.* [26] used variational mode decomposition to extract a trend and then proposed an adaptive density peaks search algorithm to realize different bearing faults. Miao *et al.* [27] constructed an convex optimization based algorithm to identify multiple states in a bearing degradation process. Miao *et al.* [28] constructed multiple filters to retain bearing fault frequencies to assess cooling fan degradation. Wang *et al.* [29] combined computed order tracking and variational mode decomposition based time frequency representation for realizing bearing fault diagnosis at variable speeds. Cui *et al.* [30] used the sparsogram and Lempel-Ziv to quantify bearing degradation. Jiang *et al.* [31] fully discussed initial parameters of variational mode decomposition for bearing fault diagnosis and proposed an optimal filtering for extracting bearing fault features. Feng *et al.* [32] proposed atomic decomposition and sparse representation to analyze planetary bearing faults.

In this paper, to further generalize the fast Kurtogram, flexible Kurtogram is proposed. Firstly, a flexible filtering framework based on multiple filter banks is constructed. Secondly, objective functions of the flexible Kurtogram based on generalized spectral kurtosis are proposed. Thirdly, optimization algorithms are introduced to maximize objective functions so as to make the flexible Kurtogram adaptive for squared envelope with demodulation analysis. The main contribution of this paper is to design adaptive filter banks used in the flexible Kurtogram, which is better than use predetermined filter banks used in the fast Kurtogram.

The rest of this paper is organized as follows. Section 2 introduces spectral kurtosis and generalized spectral kurtosis. In Section 3, the flexible Kurtogram for extracting repetitive transients is proposed. Two illustrative examples are respectively gave in Sections 4 and 5. Conclusions are drawn at last.

II. SPECTRAL KURTOSIS AND GENERALIZED SPECTRAL KURTOSIS

Spectral kurtosis was originally defined by Antoni [9] as the ratio of the raw 4th order moment m_4 to the raw 2nd order moment m_2 of an analytical signal $\overline{x_{l,h}}[n] = x_{l,h}[n] + j \cdot \text{Hilbert}\{x_{l,h}[n]\}$, where $x_{l,h}[n]$ is a filtered signal by a band-pass filter with the lower and upper cut-off frequencies l, h and Hilbert$\{\cdot\}$ is the Hilbert transform. Here, the length of the analytical signal is denoted as N. According to this definition, spectral kurtosis can be formulated as follows:

$$\kappa_{l,h}\left(\overline{x_{l,h}}[n]\right) = \frac{m_4\left\{\left|\overline{x_{l,h}}[n]\right|\right\}}{\left(m_2\left\{\left|\overline{x_{l,h}}[n]\right|\right\}\right)^2} - 2. \tag{1}$$

Further, Wang [19] decomposed spectral kurtosis as the square of the ratio of *L2* norm to *L1* norm of squared envelope (SE) $\text{SE}_{l,h}[n] = \left|\overline{x_{l,h}}[n]\right|^2$. Wang defined spectral *L2/L1*

norm as follows [15]:

$$\sqrt{N}\frac{\left\|\mathrm{SE}_{l,h}[n]\right\|_{L2}}{\left\|\mathrm{SE}_{l,h}[n]\right\|_{L1}}-\sqrt{2}, \tag{2}$$

where $\|\cdot\|_{L1}=\sum_{i=1}^{N}|x_i|$ and $\|\cdot\|_{L2}=\sqrt{\sum_{i=1}^{N}|x_i|^2}$. Then, Wang [19] thought that the ratio of *Lp* norm to *Lq* norm of SE is more general than the ratio of *L2* norm to *L1* norm of SE. Consequently, Wang defined spectral *Lp/Lq* norm as follows [19]:

$$\begin{cases} N^{1/q-1/p}\dfrac{\left\|\mathrm{SE}_{l,h}[n]\right\|_{Lp}}{\left\|\mathrm{SE}_{l,h}[n]\right\|_{Lq}}-\dfrac{\sqrt[p]{p!}}{\sqrt[q]{q!}} & p>q>0 \\[3mm] N^{-1/p}\dfrac{\left\|\mathrm{SE}_{l,h}[n]\right\|_{Lp}}{\sqrt[N]{\prod\limits_{n=1}^{N}\mathrm{SE}_{l,h}[n]}}-\dfrac{\sqrt[p]{p!}}{e^{-\gamma}} & p>q=0, \end{cases} \tag{3}$$

where the Euler-Mascheroni constant γ equals to 0.5772156649.

In (3), when $p=1$ and $q=0$, Wang showed that the ratio of *L1* norm to *L0* norm of SE equals to the reciprocal of the smoothness index. Here, the smoothness index was originally introduced by Bozchalooi and Liang [16]. Moreover, it was shown that the smoothness index is less sensitive to impulsive noises than spectral kurtosis and spectral *L2/L1* norm. In this case, the reciprocal of the smoothness index was given as follows:

$$\frac{\sum\limits_{n=1}^{N}\mathrm{SE}_{l,h}[n]\Big/N}{\sqrt[N]{\prod\limits_{n=1}^{N}\mathrm{SE}_{l,h}[n]}}-\frac{1}{e^{-\gamma}}, \quad p=1, q=0. \tag{4}$$

Consequently, (3) can be regarded as generalized spectral kurtosis in a time domain to characterize the impulsiveness of repetitive transients.

On the other hand, in some cases, impulsive noises may affect generalized spectral kurtosis in a time domain. Hence, it is necessary to characterize the cyclo-stationarity of repetitive transients. On this condition, SE needs to be mapped into a frequency domain by using the fast Fourier transform. The mapped SE is called SE spectrum (SES). Being similar with generalized spectral kurtosis in a time domain, generalized spectral kurtosis in a frequency domain is given as follows:

$$\begin{cases} N^{1/q-1/p}\dfrac{\left\|\mathrm{SES}_{l,h}[n]\right\|_{Lp}}{\left\|\mathrm{SES}_{l,h}[n]\right\|_{Lq}}-\dfrac{\sqrt[p]{p!}}{\sqrt[q]{q!}} & p>q>0 \\[3mm] N^{-1/p}\dfrac{\left\|\mathrm{SES}_{l,h}[n]\right\|_{Lp}}{\sqrt[N]{\prod\limits_{n=1}^{N}\mathrm{SES}_{l,h}[n]}}-\dfrac{\sqrt[p]{p!}}{e^{-\gamma}} & p>q=0. \end{cases} \tag{5}$$

Interestingly, when p and q are chosen as different integers, (5) are reduced to some specific theories for extracting repetitive transients. Firstly, when $p=2$ and $q=1$, (5) is

reduced to the main idea of the Sparsogram developed by Tse and Wang [33] as follows:

$$N^{1/2}\frac{\left\|\mathrm{SES}_{l,h}[n]\right\|_{L1}}{\left\|\mathrm{SES}_{l,h}[n]\right\|_{L1}}-\sqrt{2}. \tag{6}$$

Secondly, Wang *et al.* [34] clarified the relationship between the Protrugram and spectral kurtosis and discovered that the ratio of *L2* norm to *L1* norm was commonly used in these theories. Moreover, Wang et al. defined a modified Protrugram, which is a special case of (5) when $p=2$ and $q=1$ and the square operator is applied to the ratio of *L2* norm to *L1* norm of SES as follows:

$$N\frac{\left\|\mathrm{SES}_{l,h}[n]\right\|_{L1}^2}{\left\|\mathrm{SES}_{l,h}[n]\right\|_{L1}^2}-2. \tag{7}$$

Thirdly, when $p=+\infty$ and $q=1$, (5) is reduced to a cyclic harmonic to noise ratio introduced by Mo *et al.* [20]. Here, $L+\infty$ norm means to take the maximum of SES. This is reasonable because bearing fault frequency and its harmonics dominate SES when a bearing fault happens.

$$N\frac{\left\|\mathrm{SES}_{l,h}[n]\right\|_{L+\infty}}{\left\|\mathrm{SES}_{l,h}[n]\right\|_{L1}}. \tag{8}$$

III. FLEXIBLE KURTOGRAM FOR EXTRACTING REPETITIVE TRANSIENTS

In the past years, lots of algorithms have been developed to realize a special case of generalized spectral kurtosis, namely spectral kurtosis. One of the most famous realization algorithms is the fast Kurtogram [35], which used 1/3-binary tree filter banks to process a raw vibration signal and then employed kurtosis to quantify filtered signals. The maximum of kurtosis values of filtered signals on the paving of 1/3-binary tree filter banks indicates the most informative frequency band for extracting repetitive transients. The paving of 1/3-binary tree filter banks in the fast Kurtogram is plotted in Fig. 1.

In view of the paving of 1/3-binary three filter banks used in the fast Kurtogram, it is not difficult to find that the divisions of frequency bands at different decomposition levels are pre-determined and they are not adaptively determined, which indicates that such divisions may not be optimal in many cases. To solve this problem, in this paper, a flexible filtering framework is first constructed in Step 1 of the flexible Kurtogram. The divisions of frequency bands at different decomposition levels are automatically determined by maximizing objective functions in Steps 2 and 3 of the flexible Kurtogram. All steps of the proposed flexible Kurtogram are illustrated in the following.

Step 1. (Establish a Filtering Framework of the Flexible Kurtogram At A Decomposition Level M): Set a decomposition level of the flexible Kurtogram to M, which means that a normalized Fourier support $\bigcup\limits_{m=1}^{M+1}\Lambda_n=[0,\pi]$ (according to the Shannon criterion, 2π periodicity of a normalized Fourier axis is limited to $\omega\in[0,\pi]$) is divided into $M+1$ contiguous
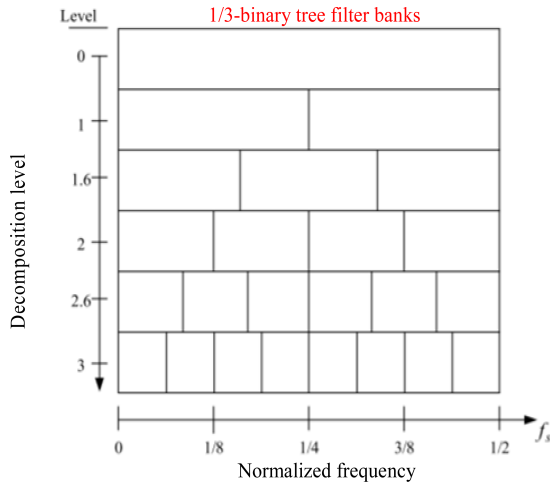
FIGURE 1. The paving of 1/3-binary tree filter banks used in the fast Kurtogram (f_S is a sampling frequency).

frequency bands $\Lambda_m = [\omega_{m-1}, \omega_m]$. The filters adopted in this paper are exactly the same filters developed by Gilles [36] as follows in (9) and (10), as shown at the bottom of this page, where $\beta(\omega) = \omega^4 (35 - 84\omega + 70\omega^2 - 20\omega^3)$ and $\gamma < \min_m \frac{(\omega_{m+1} - \omega_m)}{(\omega_{m+1} + \omega_m)}$ to make frequency supports compact. Based on (9) and (10), a signal denoted by $f(n)$ can be decomposed as follows:

$$f(n) = W_f(0, n) * \phi_1(n) + \sum_{m=1}^{M+1} W_f(m, n) * \psi_m(n)$$

$$= \text{IFT} \Bigg(\text{FT}\left(W_f(0, t)\right) \times \phi_1(\omega)$$

$$+ \sum_{m=1}^{M+1} \text{FT}\left(W_f(m, n)\right) \times \psi_m(\omega) \Bigg), \quad (11)$$

where $W_f(0, t)$ and $W_f(m, n)$ are calculated as follows:

$$W_f(0, n) = \langle f(n), \phi_1(n) \rangle$$

$$= \sum_\tau f(\tau) \overline{\phi_1(\tau - n)}$$

$$= \text{IFT} \left(\text{FT}(f(\tau)) \times \overline{\phi_1(\omega)} \right), \quad (12)$$

$$W_f(m, n) = \langle f(n), \psi_m(n) \rangle$$

$$= \sum_\tau f(\tau) \overline{\psi_m(\tau - n)}$$

$$= \text{IFT} \left(\text{FT}(f(\tau)) \times \overline{\psi_m(\omega)} \right), \quad (13)$$

where FT is the abbreviation of the fast Fourier transform and IFT is the abbreviation of the inverse Fourier transform; $*$, $\langle, \rangle$ and $\overline{()}$ are the convolution, the inner product and the complex conjugate, respectively.

Step 2 (Setting an Objective Function of the Flexible Kurtogram at a Decomposition Level M): The only problem left in Step 1 is determination of $M + 1$ contiguous frequency bands $\bigcup_{m=1}^{M+1} \Lambda_m = [0, \pi]$. To intelligently determine these frequency bands, an objective function is needed to constructed. As introduced in the previous section, generalized spectral kurtosis (3) or (5) can be used as an objective function. However, the direct use of (3) or (5) can only determine one frequency band rather than $M + 1$ contiguous frequency bands $\bigcup_{m=1}^{M+1} \Lambda_m = [0, \pi]$. Therefore, generalized spectral kurtosis (3) or (5) needs to be reformulated. An intuitive idea is to maximize the sum of generalized spectral kurtosis (3) or (5) at $M + 1$ contiguous frequency bands $\bigcup_{m=1}^{M+1} \Lambda_m = [0, \pi]$. The objective functions of the flexible Kurtogram at a decomposition level M can be formulated as (14) or (15).

The objective function of the flexible Kurtogram for characterizing the impulsiveness of repetitive transients is formulated as follows:

$$\begin{cases} \sum_{m=1}^{M+1} N^{1/q - 1/p} \dfrac{\left\| |W_f(m, n)|^2 \right\|_{Lp}}{\left\| |W_f(m, n)|^2 \right\|_{Lq}} - \dfrac{\sqrt[p]{p!}}{\sqrt[q]{q!}} & p > q > 0 \\[4ex] \sum_{m=1}^{M+1} N^{-1/p} \dfrac{\left\| |W_f(m, n)|^2 \right\|_{Lp}}{\sqrt[N]{\prod_{n=1}^{N} |W_f(m, n)|^2}} - \dfrac{\sqrt[p]{p!}}{e^{-\gamma}} & p > q = 0, \end{cases}$$

$$(14)$$

The objective function of the flexible Kurtogram for characterizing the cyclo-stationarity of repetitive transients is

$$\phi_m(\omega) = \begin{cases} 1 & |\omega| \le (1 - \gamma)\omega_m \\ \cos\left[\dfrac{\pi}{2}\beta\left(\dfrac{1}{2\gamma\omega_m}(|\omega| - (1 - \gamma)\omega_m) \right) \right] & (1 - \gamma)\omega_m \le |\omega| \le (1 + \gamma)\omega_m \\ 0 & \text{others}, \end{cases} \quad (9)$$

$$\psi_m(\omega) = \begin{cases} 1 & (1 + \gamma)\omega_m \le |\omega| \le (1 - \gamma)\omega_{m+1} \\ \cos\left[\dfrac{\pi}{2}\beta\left(\dfrac{1}{2\gamma\omega_{m+1}}(|\omega| - (1 - \gamma)\omega_{m+1}) \right) \right] & (1 - \gamma)\omega_{m+1} \le |\omega| \le (1 + \gamma)\omega_{m+1} \\ \sin\left[\dfrac{\pi}{2}\beta\left(\dfrac{1}{2\gamma\omega_m}(|\omega| - (1 - \gamma)\omega_m) \right) \right] & (1 - \gamma)\omega_m \le |\omega| \le (1 + \gamma)\omega_m \\ 0 & \text{others}, \end{cases} \quad (10)$$
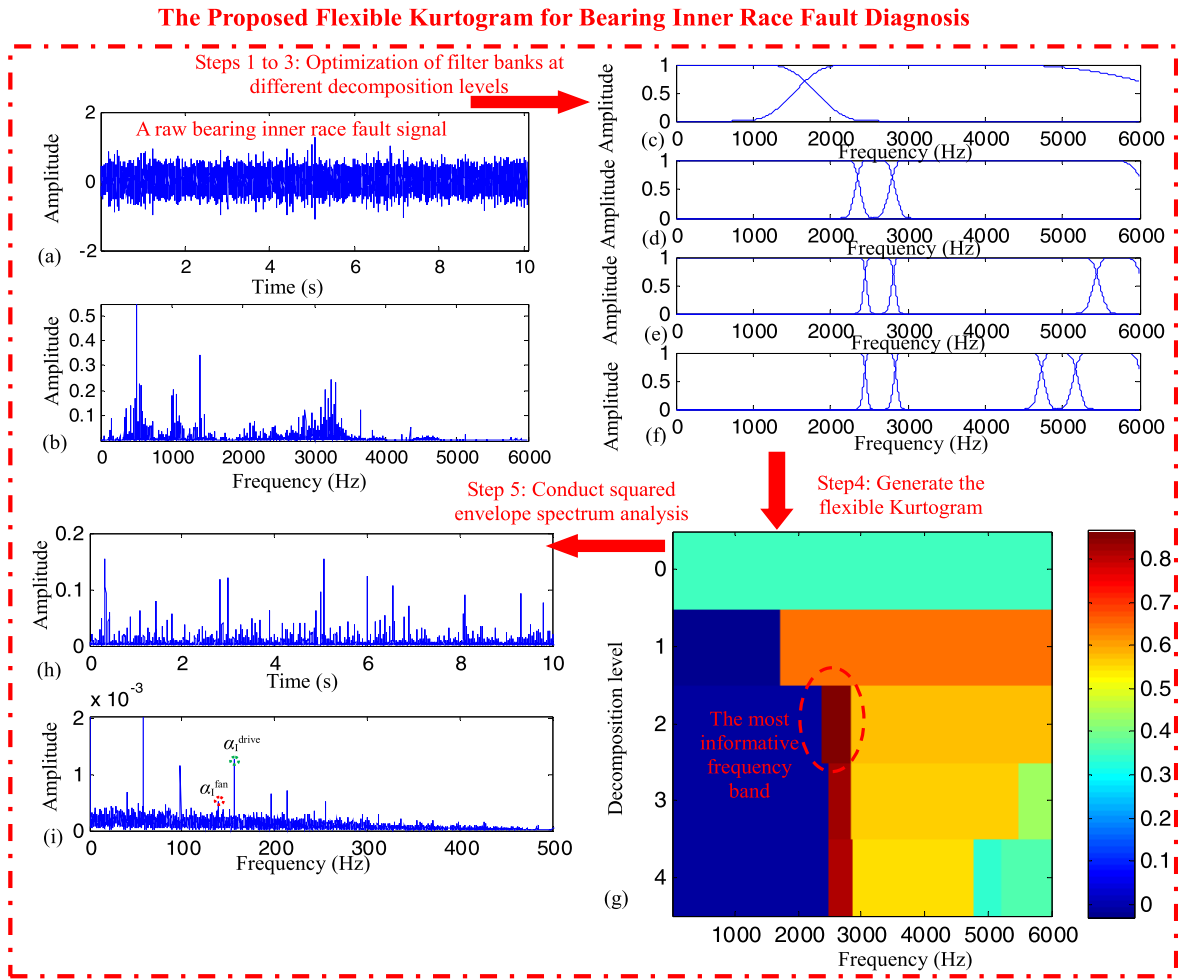
FIGURE 2. The proposed flexible Kurtogram for processing a bearing inner race fault signal: (a) a bearing inner race fault signal; (b) frequency spectrum of Fig. 2(a); (c) the optimized filter bank of the flexible Kurtogram at a decomposition level of 1; (d) the optimized filter bank of the flexible Kurtogram at a decomposition level of 2; (e) the optimized filter bank of the flexible Kurtogram at a decomposition level of 3; (f) the optimized filter bank of the flexible Kurtogram at a decomposition level of 4; (g) the flexible Kurtogram; (h) squared envelope of the most informative signal filtered by the flexible Kurtogram; (i) squared envelope spectrum of Fig. 2 (h).

formulated as follows:

$$
\begin{cases}
\sum_{m=1}^{M+1} N^{1/q-1/p} \dfrac{\left\| \left\| \mathrm{FT}\left(|W_f(m,n)|^2 \right) \right\| \right\|_{Lp}}{\left\| \left\| \mathrm{FT}\left(|W_f(m,n)|^2 \right) \right\| \right\|_{Lq}} - \dfrac{\sqrt[p]{p!}}{\sqrt[q]{q!}} & p > q > 0 \\[3ex]
\sum_{m=1}^{M+1} N^{-1/p} \dfrac{\left\| \left\| \mathrm{FT}\left(|W_f(m,n)|^2 \right) \right\| \right\|_{Lp}}{\sqrt[N]{\prod_{n=1}^{N} \left| \mathrm{FT}\left(|W_f(m,n)|^2 \right) \right|}} - \dfrac{\sqrt[p]{p!}}{e^{-\gamma}} & p > q = 0.
\end{cases}
$$

(15)

Step 3 (Solving an Objective Function of the Flexible Kurtogram at a Decomposition Level M+1 by Using an Metaheuristic Optimization Algorithm): Maximization of (14) or (15) is an optimization problem. Population-based metaheuristic optimization algorithms inspired by biological evolution can be used to solve the optimization problem. These metaheuristic optimization algorithms include ant colony optimization [37], differential evolution [38], genetic algorithm [39], particle swarm optimization [40], artificial immune systems [41], a multi-objective genetic local search algorithm [42], etc. In this paper, particle swarm optimization is used as a demonstration to maximize (14) or (15).

Firstly, some initial particles/solutions are needed to be randomly generated. Each particle/solution is a *M+1*-dimensional vector. Here, a constraint is made for maximization of (14) or (15). The constraint is $0 < \omega_1 < \ldots \omega_{m-1} < \omega_m < f_s/2$. Here, f_s is a sampling frequency. The number of particles in this paper is set to 60.

Secondly, at the kth epoch, calculate the objective function (14) or (15) of each particle/solution. If a new objective value at the current epoch is larger than the largest objective value, the current position is set to a new personal best position.

Thirdly, a particle with the largest objective value among all particles is set to the global best particle/solution. Then, suppose that $v_j(k)$ and $x_j(k)$ are the velocity and position of
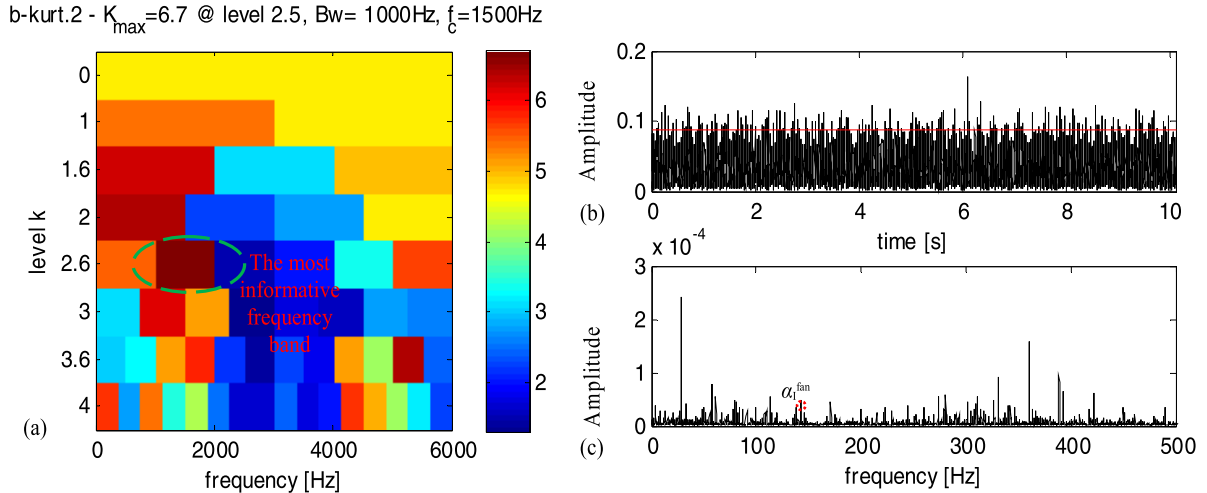
FIGURE 3. The fast Kurtogram for processing the bearing inner race fault signal: (a) the fast Kurtogram; (b) squared envelope of the most informative signal filtered by the fast Kurtogram; (c) squared envelope spectrum of Fig. 3 (b).

the jth particle/solution at the kth epoch; $p_j(k)$ is the personal best position of the jth particle/solution at the kth epoch; $g(k)$ is the global best position at the kth epoch. (16) and (17) are used to update the position of each particle/solution at the $k + 1^{\text{th}}$ epoch.

$$v_j(k+1) = v_j(k) + r_1 c_1 \left(p_j(k) - x_j(k) \right)$$
$$+ r_2 c_2 \left(g(k) - x_j(k) \right), \quad (16)$$
$$x_j(k+1) = x_j(k) + v_j(k+1), \quad (17)$$

where r_1 and r_2 are two random numbers between 0 to 1; c_1 and c_2 are respectively a cognitive weight and a social weight. In this paper, $c_1 = c_2 = 2$.

Repeat these procedures until a maximum number of epochs is achieved. In this paper, the maximum number of epochs is set to 100.

Step 4 (Generate the Flexible Kurtogram at Different Decomposition Levels): Repeat Steps 1 to 3 to generate the paving of the flexible Kurtogram from decomposition levels 1 to $M + 1$.

Step 5: Use the maximum of the flexible Kurtogram as a criterion to choose the most informative frequency band and then conduct squared envelope analysis to identify various bearing fault frequencies.

IV. THE FIRST ILLUSTRATE EXAMPLE

In this section, analyses of an inner race fault at a fan end of a motor (file name: 277DE of Case Western Reserve University datasets, a partially successful case [43] suggested by Smith and Randall; $f_s = 12000$ Hz; a rotation frequency $\alpha_s = 28.9$ Hz; a bearing inner race fault frequency $\alpha_I^{\text{fan}} = 142.9$ at a fan end of a motor; a bearing inner race fault frequency $\alpha_I^{\text{drive}} = 156.4$ at a drive end of a motor) is used as an example to illustrate the procedure of the flexible Kurtogram in Fig. 2. Besides, to reduce the length of this paper, $p = 2$ and $q = 1$ (the ratio of *L2* norm to *L1* norm) as a special case of (14) is used as an objective function.

In this example, the difficulty of bearing fault detection is caused by an accelerometer installed at a drive-end bearing. In Fig. 2, it is clearly seen that the filter banks used in the flexible Kurtogram are automatically optimized at different decomposition levels. Moreover, the most informative frequency band indicated by the flexible Kurtogram results in a squared envelope spectrum that exhibits the bearing inner race fault frequency $\alpha_I^{\text{fan}} = 142.9$ at the fan end and the bearing inner race fault frequency $\alpha_I^{\text{drive}} = 156.4$ at the drive end, which indicates that the proposed flexible Kurtogram can simultaneously detect two bearing inner race faults at the different ends of the motor, which is partially successfully in [43] by using various fault detection techniques.

Further, to highlight the superiority of the proposed flexible Kurtogram, a comparison with the fast Kurtogram is conducted. The results obtained by using the fast Kurtogram are plotted in Fig. 3, where it is found that the fast Kurtogram can only detect $\alpha_I^{\text{fan}} = 142.9$ at the fan end. Therefore, the fast Kurtogram also belongs to one of the partly successful fault detection techniques.

V. THE SECOND ILLUSTRATE EXAMPLE

The second example is about analyses of a bearing ball fault signal collected from a motor. The raw bearing ball fault signal is available in [44]. In the experiment, the shaft rotation frequency $f_r = 23.33$ Hz, the sampling frequency $f_s = 80$ kHz; the bearing ball spinning frequency $\alpha_B = 64$ Hz and the cage frequency $\alpha_C = 9.7$. Firstly, the flexible Kurtogram is applied to process the bearing ball fault signal. The results obtained by using the flexible Kurtogram is shown in Fig. 4, where it is observed that the flexible Kurtogram can locate the most informative frequency band at decomposition level 4. The bearing ball spinning frequency, its harmonics and the cage frequency can be clearly detected in Fig. 4 (i), which are typical fault symptoms for a bearing ball fault. Therefore, the bearing ball fault can
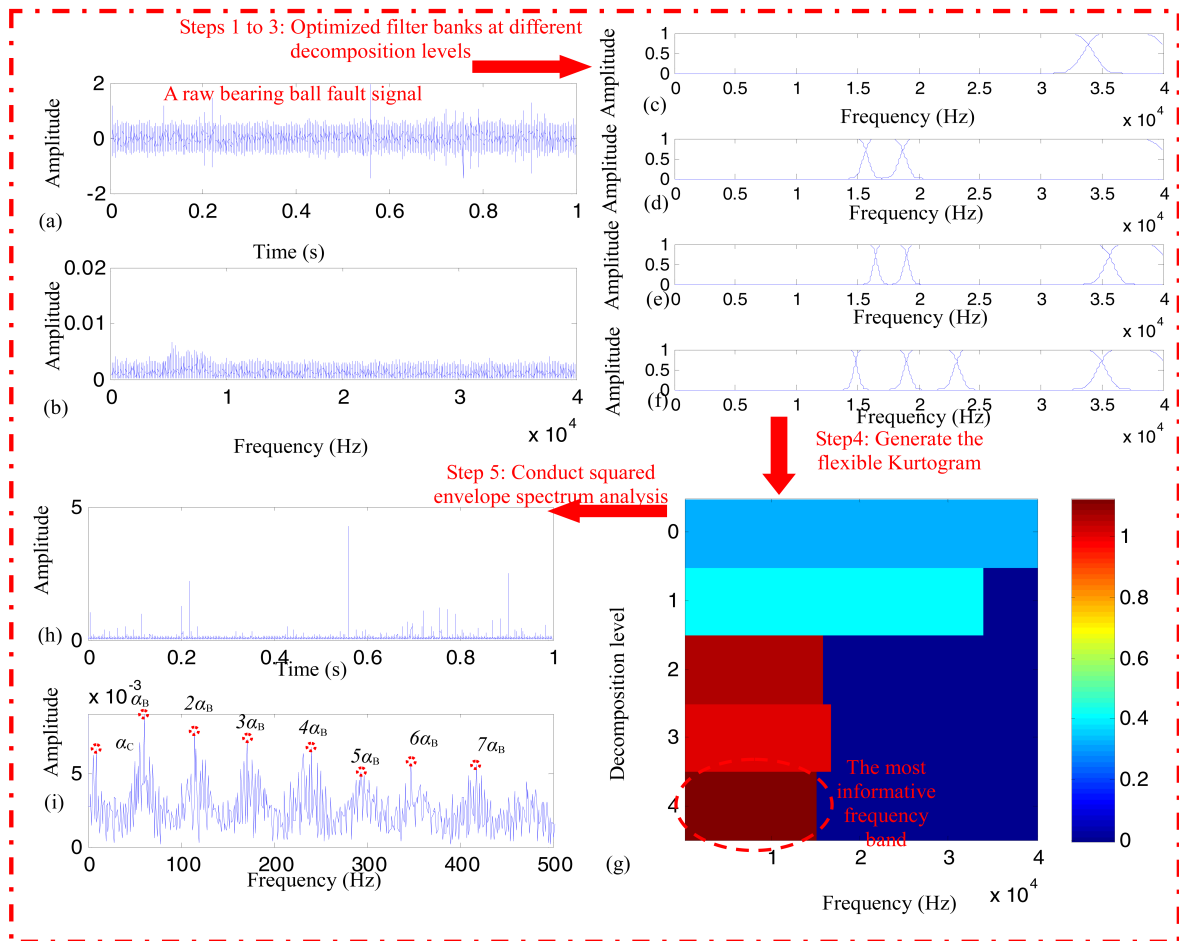
FIGURE 4. The proposed flexible Kurtogram for processing a bearing ball fault signal: (a) a bearing ball fault signal; (b) frequency spectrum of Fig. 4 (a); (c) the optimized filter bank of the flexible Kurtogram at a decomposition level of 1; (d) the optimized filter bank of the flexible Kurtogram at a decomposition level of 2; (e) the optimized filter bank of the flexible Kurtogram at a decomposition level of 3; (f) the optimized filter bank of the flexible Kurtogram at a decomposition level of 4; (g) the flexible Kurtogram; (h) squared envelope of the most informative signal filtered by the flexible Kurtogram; (i) squared envelope spectrum of Fig. 4 (h).
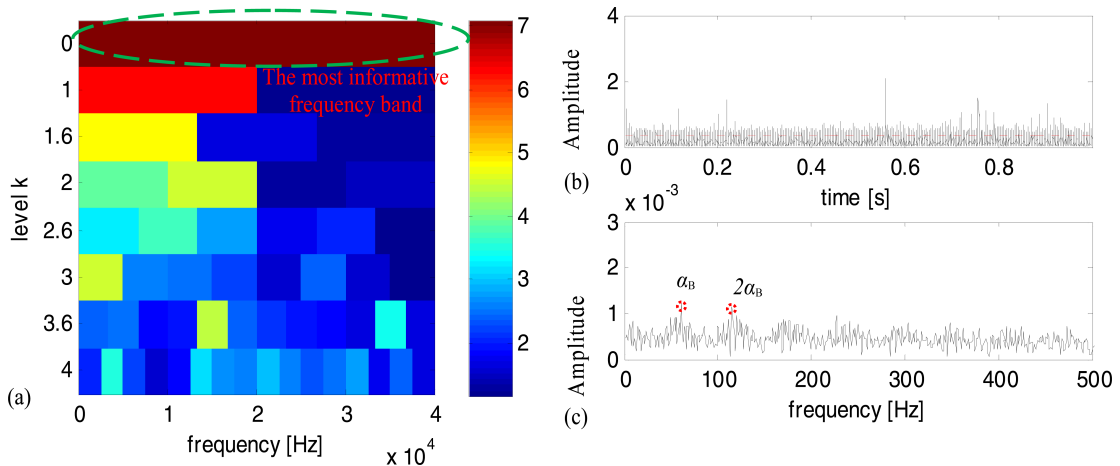

FIGURE 5. The fast Kurtogram for processing the bearing ball fault signal: (a) the fast Kurtogram; (b) squared envelope of the most informative signal filtered by the fast Kurtogram; (c) squared envelope spectrum of Fig. 5(b).

be confirmed. For a comparison, the fast Kurtogram is applied to process the same bearing ball fault signal. The results obtained by using the fast Kurtogram is shown in Fig. 5, where it is indicated that the whole fault signal is the most informative. In Fig. 5 (c), the cage frequency is not as clear as that shown in Fig. 4 (i). Moreover, the harmonics of the ball

spinning frequency are not as clear as those shown in Fig. 4(i). This is because the whole bearing ball fault signal is used in squared envelope analysis. As shown in Fig. 4(b), many noises corrupt the frequency spectrum of the bearing ball fault signal. In contrast, the flexible Kurtogram can find the optimal band-pass filter to retain bearing ball fault signatures.

VI. CONCLUSION

In this paper, to make the fast Kurtogram adaptive, the flexible Kurtogram was proposed accordingly. The main idea of the flexible Kurtogram is to optimize the filter banks. Firstly, a filtering bank framework at different decomposition levels was constructed. Secondly, based on generalized spectral kurtosis in time and frequency domain, two objective functions were respectively designed to characterize the impulsiveness and the cyclo-stationarity of repetitive transients. So, maximization of the proposed objective functions can be used to automatically determine the filter banks at different decomposition levels required in the flexible Kurtogram. Thirdly, evolutionary optimization algorithms were introduced to maximize the proposed objective functions. Two illustrative examples were provided. In the first illustrative example, it was found that the proposed flexible Kurtogram can simultaneously detect two bearing inner race faults at the two different ends of a motor, while the fast Kurtogram can only detect one fault. In the second illustrative example, it was found that the filter bank at decomposition level 4 locates the most informative frequency band for further squared envelope with demodulation analysis and improve the signal to noise ratio of squared envelope spectrum for bearing ball fault diagnosis, while the fast Kurtogram can only indicates the whole frequency band, resulting in the unclear cage frequency in its corresponding frequency spectrum in Fig. 5(c).

REFERENCES

[1] M. Cerrada *et al.*, "A review on data-driven fault severity assessment in rolling bearings," *Mech. Syst. Signal Process.*, vol. 99, pp. 169–196, Jan. 2018.

[2] C. Li, J. L. van der Oliveira, M. C. Lozada, D. Cabrera, V. Sanchez, and G. Zurita, "A systematic review of fuzzy formalisms for bearing fault diagnosis," *IEEE Trans. Fuzzy Syst.*, to be published.

[3] X. Guo, L. Chen, and C. Shen, "Hierarchical adaptive deep convolution neural network and its application to bearing fault diagnosis," *Measurement*, vol. 93, pp. 490–502, Nov. 2016.

[4] Y. Lei, N. Li, L. Guo, N. Li, T. Yan, and J. Lin, "Machinery health prognostics: A systematic review from data acquisition to RUL prediction," *Mech. Syst. Signal Process.*, vol. 104, pp. 799–834, May 2018.

[5] C. Shen, D. Wang, F. Kong, and P. W. Tse, "Fault diagnosis of rotating machinery based on the statistical parameters of wavelet packet paving and a generic support vector regressive classifier," *Measurement*, vol. 46, no. 4, pp. 1551–1564, May 2013.

[6] D. Wang, K. Tsui, and Q. Miao, "Prognostics and health management: A review of vibration based bearing and gear health indicators," *IEEE Access*, vol. 6, pp. 665–676, 2018.

[7] D. Wang and K. Tsui, "Statistical modeling of bearing degradation signals," *IEEE Trans. Rel.*, vol. 66, no. 4, pp. 1331–1344, Dec. 2017.

[8] Y. Yang, Z. Peng, and W. Zhang, "Parameterised time-frequency analysis methods and their engineering applications: A review of recent advances," *Mech. Syst. Signal Process.*, vol. 119, pp. 182–221, 2019.

[9] J. Antoni, "The spectral kurtosis: A useful tool for characterising non-stationary signals," *Mech. Syst. Signal Process.*, vol. 20, no. 2, pp. 282–307, Feb. 2006.

[10] J. Antoni and R. Randall, "The spectral kurtosis: Application to the vibratory surveillance and diagnostics of rotating machines," *Mech. Syst. Signal Process.*, vol. 20, no. 2, pp. 308–331, 2006.

[11] J. Antoni, G. Xin, and N. Hamzaoui, "Fast computation of the spectral correlation," *Mech. Syst. Signal Process.*, vol. 92, pp. 248–277, Aug. 2017.

[12] Y. Wang, J. Xiang, R. Markert, and M. Liang, "Spectral kurtosis for fault detection, diagnosis and prognostics of rotating machines: A review with applications," *Mech. Syst. Signal Process.*, vol. 66, pp. 679–698, Jan. 2016.

[13] C. Li, D. Cabrera, J. V. de Oliveira, R.-V. Sanchez, M. Cerrada, and G. Zurita, "Extracting repetitive transients for rotating machinery diagnosis using multiscale clustered grey infogram," *Mech. Syst. Signal Process.*, vol. 76, pp. 157–173, Aug. 2016.

[14] P. Borghesani, P. Pennacchi, and S. Chatterton, "The relationship between kurtosis- and envelope-based indexes for the diagnostic of rolling element bearings," *Mech. Syst. Signal Process.*, vol. 43, no. 1, pp. 25–43, Feb. 2014.

[15] D. Wang, "Spectral L2/L1 norm: A new perspective for spectral kurtosis for characterizing non-stationary signals," *Mech. Syst. Signal Process.*, vol. 104, pp. 290–293, May 2018.

[16] I. S. Bozchalooi and M. Liang, "A smoothness index-guided approach to wavelet parameter selection in signal de-noising and fault detection," *J. Sound Vib.*, vol. 308, nos. 1–2, pp. 246–267, Nov. 2007.

[17] H. Dalton, "The measurement of the inequality of incomes," *Econ. J.*, vol. 30, no. 119, pp. 348–361, Sep. 1920.

[18] Y. Miao, M. Zhao, and J. Lin, "Improvement of kurtosis-guided-grams via Gini index for bearing fault feature identification," *Meas. Sci. Technol.*, vol. 28, Nov. 2017, Art. no. 125001.

[19] D. Wang, "Some further thoughts about spectral kurtosis, spectral L2/L1 norm, spectral smoothness index and spectral Gini index for characterizing repetitive transients," *Mech. Syst. Signal Process.*, vol. 108, pp. 360–368, Aug. 2018.

[20] Z. Mo, J. Wang, H. Zhang, and Q. Miao, "Weighted cyclic harmonic-to-noise ratio for rolling element bearing fault diagnosis," *IEEE Trans. Instrum. Meas.*, to be published.

[21] T. Barszcz and A. Jabłoński, "A novel method for the optimal band selection for vibration signal demodulation and comparison with the Kurtogram," *Mech. Syst. Signal Process.*, vol. 25, no. 1, pp. 431–451, 2011.

[22] D. Wang, P. W. Tse, and K. L. Tsui, "An enhanced Kurtogram method for fault diagnosis of rolling element bearings," *Mech. Syst. Signal Process.*, vol. 35, nos. 1–2, pp. 176–199, Feb. 2013.

[23] J. Antoni, "The infogram: Entropic evidence of the signature of repetitive transients," *Mech. Syst. Signal Process.*, vol. 74, pp. 73–94, Jun. 2016.

[24] M. Wang, Z. Mo, H. Fu, H. Yu, and Q. Miao, "Harmonic L2/L1 norm for bearing fault diagnosis," *IEEE Access*, vol. 7, pp. 27313–27321, 2019.

[25] Y. Qin, "a new family of model-based impulsive wavelets and their sparse representation for rolling bearing fault diagnosis," *IEEE Trans. Ind. Electron.*, vol. 65, no. 3, pp. 2716–2726, Mar. 2018.

[26] Y. Wang, Z. Wei, and J. Yang, "Feature trend extraction and adaptive density peaks search for intelligent fault diagnosis of machines," *IEEE Trans. Ind. Informat.*, vol. 15, no. 1, pp. 105–115, Jan. 2019.

[27] Q. Miao, X. Zhang, Z. Liu, and H. Zhang, "Condition multi-classification and evaluation of system degradation process using an improved support vector machine," *Microelectron. Rel.*, vol. 75, pp. 223–232, Aug. 2017.

[28] Q. Miao, C. Tang, W. Liang, and M. Pecht, "Health assessment of cooling fan bearings using wavelet-based filtering," *Sensors*, vol. 13, no. 1, pp. 274–291, Dec. 2012.

[29] Y. Wang, L. Yang, J. Xiang, J. Yang, and S. He, "A hybrid approach to fault diagnosis of roller bearings under variable speed conditions," *Meas. Sci. Technol.*, vol. 28, no. 12, 2017, Art. no. 125104.

[30] L. Cui, B. Li, J. Ma, and Z. Jin, "Quantitative trend fault diagnosis of a rolling bearing based on sparsogram and Lempel-Ziv," *Measurement*, vol. 128, pp. 410–418, Nov. 2018.

[31] X. Jiang, C. Shen, J. Shi, and Z. Zhu, "Initial center frequency-guided VMD for fault diagnosis of rotating machines," *J. Sound Vib.*, vol. 435, pp. 36–55, Nov. 2018.

[32] Z. Feng, Y. Zhou, M. J. Zuo, F. Chu, and X. Chen, "Atomic decomposition and sparse representation for complex signal analysis in machinery fault diagnosis: A review with examples," *Measurement*, vol. 103, pp. 106–132, Jun. 2017.

[33] P. W. Tse and D. Wang, "The design of a new sparsogram for fast bearing fault diagnosis: Part 1 of the two related manuscripts that have a joint title as 'Two automatic vibration-based fault diagnostic methods using the novel sparsity measurement—Parts 1 and 2,'" *Mech. Syst. Signal Process.*, vol. 40, pp. 499–519, Nov. 2013.

[34] D. Wang, X. Zhao, L.-L. Kou, Y. Qin, Y. Zhao, and K.-L. Tsui, "A simple and fast guideline for generating enhanced/squared envelope spectra from spectral coherence for bearing fault diagnosis," *Mech. Syst. Signal Process.*, vol. 122, pp. 754–768, May 2019.

[35] J. Antoni, "Fast computation of the kurtogram for the detection of transient faults," *Mech. Syst. Signal Process.*, vol. 21, no. 1, pp. 108–124, 2007.

[36] J. Gilles, "Empirical wavelet transform," *IEEE Trans. Signal Process.*, vol. 61, no. 16, pp. 3999–4010, Aug. 2013.

[37] M. Dorigo, M. Birattari, and T. Stutzle, "Ant colony optimization," *IEEE Comput. Intell. Mag.*, vol. 1, no. 4, pp. 28–39, Nov. 2006.

[38] S. Das and P. N. Suganthan, "Differential evolution: A survey of the state-of-the-art," *IEEE Trans. Evol. Comput.*, vol. 15, no. 1, pp. 4–31, Feb. 2011.

[39] K. Deb, A. Pratap, S. Agarwal, and T. Meyarivan, "A fast and elitist multiobjective genetic algorithm: NSGA-II," *IEEE Trans. Evol. Comput.*, vol. 6, no. 2, pp. 182–197, Apr. 2002.

[40] J. Kennedy and R. Eberhart, "Particle swarm optimization," in *Proc. Int. Conf. Neural Netw.*, Nov. 2002, pp. 1942–1948.

[41] L. N. de Castro and J. I. Timmis, "Artificial immune systems as a novel soft computing paradigm," *Soft Comput.*, vol. 7, no. 8, pp. 526–544, 2003.

[42] L. Jianyu, S. Zhenzhong, P. M. Pardalos, H. Ying, Z. Shaohui, and L. Chuan, "A hybrid multi-objective genetic local search algorithm for the prize-collecting vehicle routing problem," *Inf. Sci.*, vol. 478, pp. 40–61, Apr. 2019.

[43] W. A. Smith and R. B. Randall, "Rolling element bearing diagnostics using the Case Western Reserve University data: A benchmark study," *Mech. Syst. Signal Process.*, vol. 64, pp. 100–131, Dec. 2015.

[44] D. Wang and K.-L. Tsui, "Dynamic Bayesian wavelet transform: New methodology for extraction of repetitive transients," *Mech. Syst. Signal Process.*, vol. 88, pp. 137–144, May 2017.

Authors' photographs and biographies not available at the time of publication.

• • •